Research Article Vol. 2, No. 2 / 25 April 2024 / Optica Quantum 57

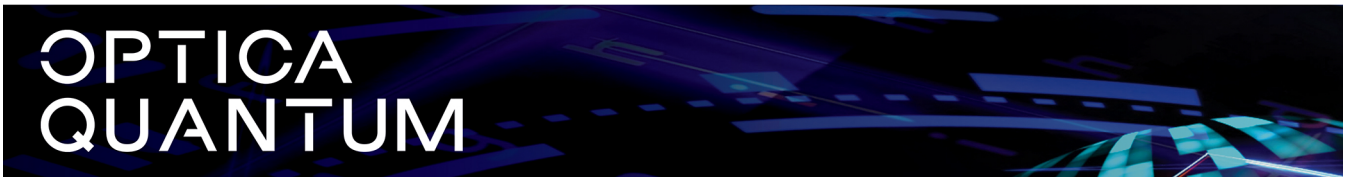

Harnessing quantum emitter rings for efficient energy transport and trapping

Raphael Holzinger,[1,*] Jonah S. Peter,[2,3] Stefan Ostermann,[2] Helmut Ritsch,[1] and Susanne Yelin[2]

[1] Institute for Theoretical Physics, University of Innsbruck, Technikerstrasse 21a, A-6020 Innsbruck, Austria
[2] Department of Physics, Harvard University, Cambridge, Massachusetts 02138, USA
[3] Biophysics Program, Harvard University, Boston, Massachusetts 02115, USA
*raphael.holzinger@uibk.ac.at

Received 30 October 2023; revised 28 January 2024; accepted 29 January 2024; published 7 March 2024

Efficient transport and harvesting of excitation energy under low light conditions is an important process in nature and quantum technologies alike. Here we formulate a quantum optics perspective to excitation energy transport in configurations of two-level quantum emitters with a particular emphasis on efficiency and robustness against disorder. We study a periodic geometry of emitter rings with subwavelength spacing, where collective electronic states emerge due to near-field dipole–dipole interactions. The system gives rise to collective subradiant states that are particularly suited to excitation transport and are protected from energy disorder and radiative decoherence. Comparing ring geometries with other configurations shows that the former are more efficient in absorbing, transporting, and trapping incident light. Because our findings are agnostic as to the specific choice of quantum emitters, they indicate general design principles for quantum technologies with superior photon transport properties and may elucidate potential mechanisms resulting in the highly efficient energy transport efficiencies in natural light-harvesting systems.

https://doi.org/10.1364/OPTICAQ.510021

1. INTRODUCTION

In quantum optics, ordered quantum emitter lattices with subwavelength spacing have emerged as a resourceful platform for near-term quantum technologies [1–12]. Here long-range interactions between light-induced dipoles lead to highly modified optical properties of the quantum emitter ensemble, including Dicke superradiance [13] and the emergence of collective long-lived subradiant states [14,15]. Applications range from single-photon switch gates [16] to enhanced single-photon detection for biomedical applications [17,18] and topological edge state lasing [19,20]. Likewise, uncovering design principles underlying biological systems and applying this understanding to synthetic systems is crucial for near-term quantum technologies. Ring geometries of quantum emitters promise to enhance single-photon sensing, transport, storage, and light generation in engineered nanoscale systems [15,21–23]. In photosynthetic energy transfer, as it occurs in nature, organisms use ring-shaped antennae that increase the photon scattering cross section of a single reaction center: the site where photosynthesis takes place. This transfer process occurs at near unit efficiency, and understanding the mechanisms behind this remarkable feat is an outstanding scientific challenge [24–34].

Taking inspiration from biological systems, we examine the long-range excitation transport between a donor and an acceptor emitter through a lattice of quantum emitter rings [Fig. 1(a)]. As a main result, we show that efficient excitation transport at low trapping rates preferentially occurs for ring geometries, as compared with other lattices. This property has important consequences for devising artificial light harvesting and transport systems, and may be relevant for understanding the excellent excitation transport capabilities of biological systems [35]. We also highlight that for ring lattices, the trapping of light at an acceptor site under low-light conditions is enhanced by many orders of magnitude as compared to other geometries and to independent emitters. By choosing an optimal detuning for the donor and acceptor with respect to the lattice, radiative losses are strongly suppressed, and excitations are protected during the transport by subradiance [14,15]. While the influence of the excitation trapping rate on the transport efficiency in other geometries has been explored in other works [36–39], as have certain design principles for bio-inspired artificial solar-harvesting devices [24,26,27,40–44], our findings specifically highlight the advantages of the rotationally symmetric ring geometry. This special feature of ring configurations is particularly intriguing for its close connection to natural photosynthetic complexes found in biological systems. Our work therefore opens the possibility of exploiting quantum effects in bio-inspired configurations of quantum emitters for near-term optical technologies that enable quantum-enhanced light–matter coupling on the nanoscale.

2. QUANTUM OPTICAL MODEL

As a paradigmatic quantum optical model to simulate excitation energy transport, we consider a one-dimensional lattice of M rotationally symmetric rings, each composed of N_R identical two-level emitters with a ground state $|g\rangle$ and an excited state $|e\rangle$. The two states are connected via the transition operator $\hat{\sigma}_n = |g_n\rangle\langle e_n|$ for the nth emitter. Additional emitters acting as donor and acceptor sites are placed in the center of two rings at either end of the lattice, as illustrated in Fig. 1(a). The transport efficiency between these two sites is the core quantity of interest and is defined as

$$\eta_t = \Gamma_{\mathrm{T}} \int_0^t dt' \langle \Psi(t')|\hat{\sigma}_{\mathrm{a}}^{\dagger}\hat{\sigma}_{\mathrm{a}}|\Psi(t')\rangle. \tag{1}$$

Here t is the integration time over which excitation can accumulate in the trap state [see Fig. 1(a)], η_t can take values between 0 and 1, where 0 corresponds to no transport at all and 1 identifies maximal transport efficiency, and $\hat{\sigma}_a^{\dagger}\hat{\sigma}_a = |e_a\rangle\langle e_a|$ corresponds to the projector onto the excited state of the acceptor. The trap population accumulates over time and reaches a steady-state value at large times t when the total excited state population is either dissipated via radiative losses or accumulated in the trap. The transition frequencies and decay rates of the ring emitters are assumed to be equal and given by $\omega_0 = 2\pi c/\lambda_0$ and

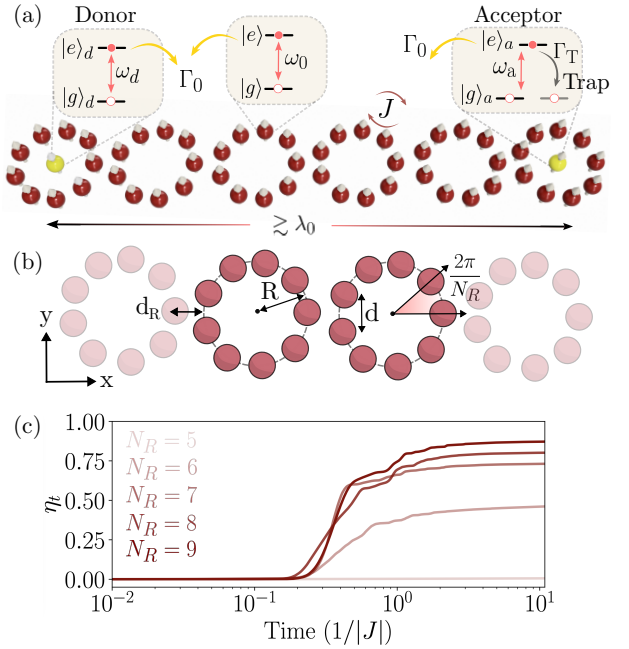

Fig. 1. Lattices of nanoscopic quantum emitter rings. (a) Each ring is composed of two-level quantum emitters with resonance frequency ω_0 and separation $d<\lambda_0$, where $\lambda_0 = \omega_0/c$ is the wavelength of light. The excited state $|e\rangle$ spontaneously decays with rate Γ_0 to the ground state $|g\rangle$ and the emitters are coupled via long-range dipole–dipole interactions with nearest-neighbor coupling strength J. Emitters acting as donor and acceptor are shown in yellow and the acceptor features an additional trapping state to which excitations irreversibly decay with rate Γ_{T}. (b) More detailed sketch illustrating the inter-ring separation d_R. The ring radius R and the emitter spacing d are related via $d = 2R\sin(\pi/N_{\mathrm{R}})$, with N_R emitters per ring. (c) Excitation transport efficiency according to Eq. (1) for a chain of 10 rings and various N_R. Parameters: $d/\lambda_0 = 0.05$, $d_R/d = 0.9$, $\Gamma_{\mathrm{T}}/\Gamma_0 = 2$, and $\Delta = 0$.

Γ_0, respectively, whereas the donor/acceptor transitions may be detuned by $\Delta = \omega_{\mathrm{d,a}} - \omega_0$ with respect to the ring emitter frequencies. We assume $\omega_{\mathrm{d}} = \omega_{\mathrm{a}}$ for the remainder of this work. The acceptor features an extra trapping channel through which excitations are extracted from the system at a rate Γ_{T}. Furthermore, the quantum emitters are confined in the x–y plane with intra-ring separation $d = 2R\sin(\pi/N_R)$ and inter-ring separation d_R, where R is the ring radius, as illustrated in Fig. 1(b). To reduce the number of free parameters, all dipole emitters are assumed to be circular polarized, namely $(1, i, 0)^T/\sqrt{2}$. However, qualitatively similar results can be obtained for geometries consisting of linear polarized emitters.

We model the system within the Born–Markov approximation [14], and only consider the quantum emitter's internal degrees of freedom. Furthermore, we assume the weak excitation regime, where at most a single excitation is present in the system (see Supplement 1 for details), and therefore the system can be described (in the rotating frame with ω_0) by the non-Hermitian Hamiltonian $\hat{\mathcal{H}}_{\mathrm{eff}} = \hat{\mathcal{H}}_{\mathrm{ad}} + \hat{\mathcal{H}}_{\mathrm{lattice}} + \hat{\mathcal{H}}_{\mathrm{int}}$. Here, $\hat{\mathcal{H}}_{\mathrm{ad}} = (\Delta - \frac{i}{2}\Gamma_0)(\hat{\sigma}_{\mathrm{a}}^{\dagger}\hat{\sigma}_{\mathrm{a}} + \hat{\sigma}_{\mathrm{d}}^{\dagger}\hat{\sigma}_{\mathrm{d}}) - \frac{i}{2}\Gamma_{\mathrm{T}}\hat{\sigma}_{\mathrm{a}}^{\dagger}\hat{\sigma}_{\mathrm{a}}$ is the bare Hamiltonian of the donor and acceptor, $\hat{\mathcal{H}}_{\mathrm{lattice}}$ describes the emitters in the ring lattice, and $\hat{\mathcal{H}}_{\mathrm{int}}$ describes the interaction between the ring emitters and the donor/acceptor,

$$\hat{\mathcal{H}}_{\mathrm{lattice}} = \sum_{n,m}\left(J_{nm} - i\frac{\Gamma_{nm}}{2}\right)\hat{\sigma}_n^{\dagger}\hat{\sigma}_m, \tag{2a}$$

$$\hat{\mathcal{H}}_{\mathrm{int}} = \sum_{n;k=\mathrm{a,d}}\left(J_{nk} - i\frac{\Gamma_{nk}}{2}\right)(\hat{\sigma}_n^{\dagger}\hat{\sigma}_k + \hat{\sigma}_k^{\dagger}\hat{\sigma}_n). \tag{2b}$$

All emitters interact via vacuum-mediated dipole–dipole interactions in free space. The pairwise coherent and dissipative interactions are given by $J_{nm} = -3\pi\Gamma_0/k_0\ \mathrm{Real}(G_{nm})$ and $\Gamma_{nm} = 6\pi\Gamma_0/k_0\ \mathrm{Imag}(G_{nm})$, respectively, with G_{nm} being the free space Green's function (see Supplement 1 for details). The Green's function depends only on the separations between the emitters and their dipole orientation. The time evolution of the system is described by the effective Hamiltonian in Eq. (2) via the Schrödinger equation $i\partial_t|\Psi(t)\rangle = \hat{\mathcal{H}}_{\mathrm{eff}}|\Psi(t)\rangle$. Since the Hamiltonian is non-Hermitian, the amplitude of the wavefunction for the quantum emitters decreases with time, which is a direct manifestation of the dissipative nature of the system.

3. COLLECTIVE MODES

As discussed in previous works [14,15,21], a subwavelength-spaced ring of quantum emitters exhibits guided eigenmodes that are extremely subradiant, exhibiting an exponentially increasing lifetime, $\tau\Gamma_0 \sim \exp(N_R)$, of a single excitation [21]. Aside from the bright symmetric superposition state, the fields of the remaining eigenmodes vanish at the center of the ring due to symmetry. Thus, they are decoupled from any emitter at the center. Here we demonstrate that a donor/acceptor at the center of the ring that is dipole–dipole coupled to the symmetric ring mode can form a subradiant state with a majority of the excitation concentrated in the donor/acceptor. We start by analyzing a single ring of N_R emitters with a single donor in the center. For a single ring, where the dipole orientations preserve the discrete rotational invariance, the collective eigenmodes of the effective Hamiltonian are spin waves of the form $|\Psi_m\rangle = \hat{S}_m^{\dagger}|G\rangle$, where

$$\hat{S}_m = \frac{1}{\sqrt{N_R}}\sum_{j=1}^{N_R} e^{im\varphi_j}\hat{\sigma}_j \tag{3}$$

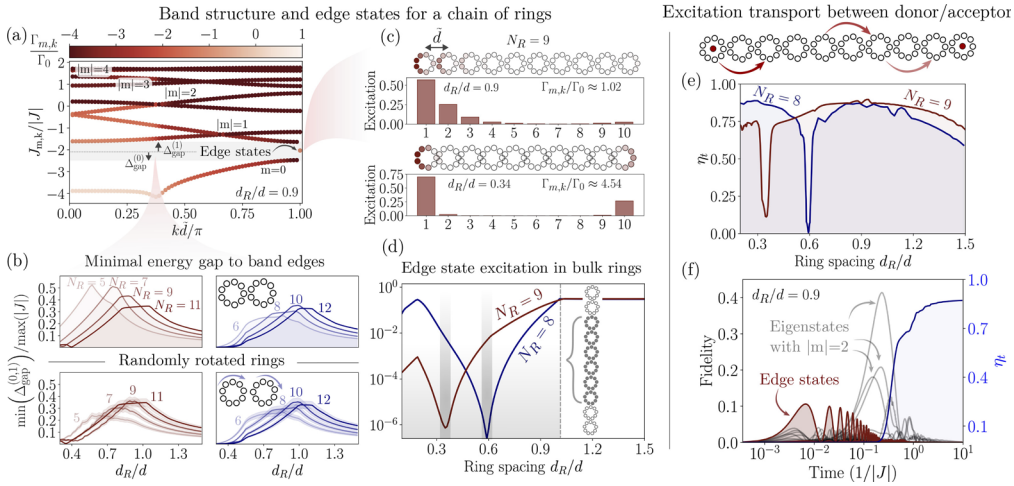

Fig. 2. Band structure, edge states, and excitation transport for a chain of rings. (a) Eigenmodes of the effective Hamiltonian $\hat{\mathcal{H}}_{\text{lattice}}$ in Eq. (2a) can be cast into $N_R = 9$ energy bands with an angular momentum projection $|m|$ using the Ansatz shown in Supplement 1 and translation along the ring chain axis is given by $\tilde{d} = 2R + d_R$, the spacing between adjacent ring centers. (Decay rates of all eigenmodes are color coded.) A band gap emerges with two edge states residing inside with an energy separation $\Delta_{\text{gap}}^{(0,1)}$ to the nearest lower/upper band edge respectively. (b) Minimal energy gap $\Delta_{\text{gap}}^{(0,1)}$ to the nearest lower/upper band edge normalized by the maximal nearest-neighbor coupling J shows distinct maxima as a function of d_R. These maxima correspond to an optimal transport efficiency η_t as shown in panel (e) for $N_R = 8, 9$. Furthermore, smaller emitter numbers per ring N_R are affected more by randomly rotated rings except for even N_R. The average was taken over 50 random realizations and where the rings can be randomly rotated between $\pm 2\pi/N_R$. (c) For $N_R = 9$, edge states appear with maximum amplitude on the left/right end of the ring chain and a superradiant decay rate for decreasing inter-ring spacings d_R/d. Notably, topological edge states have been observed in zigzag chains of gold nano-rings [19,20] with lasing from the edge rings. (d) With decreasing inter-ring spacing d_R, edge states become more pronounced with distinct minima where the bulk amplitude vanishes leading to a suppression of excitation transport. (e) Excitation transport between a donor and acceptor site placed in the center of the edge rings. The transport efficiency η_t is evaluated after a time $t\Gamma_0 = 150$ with the donor/acceptor detuning Δ optimized for maximum transport. Suppression appears when the edge states become too pronounced with vanishing amplitude in the bulk rings as shown in panel (d). (f) Time dynamics of the excitation transport process between a donor and acceptor site with $\Delta = 0$. The eigenstate fidelity $|\langle\Psi(t)|\Psi_{\text{eig}}\rangle|^2$ for $N_R = 9$ demonstrates the importance of edge states at early times. Parameters: $d = 0.05\lambda_0$, $\Gamma_T/\Gamma_0 = 1$ in panels (e),(f) and 10 rings in panels (b)–(f).

and $|G\rangle$ denotes all emitters in the ground state. Here $\varphi_j = 2\pi j/N_R$ is the angle between neighboring emitters along the ring and $m = 0, \pm 1, \cdots, \lceil \pm (N_R - 1)/2 \rceil$ is the angular momentum of the collective mode. The associated energy shifts and decay rates of these spin waves are given by $\tilde{J}_m = \sum_j e^{im\varphi_j} J_{1j}$ and $\tilde{\Gamma}_m = \sum_j e^{im\varphi_j} \Gamma_{1j}$, respectively. In such a configuration, all ring emitters couple equally to the central donor, which restricts the spectrum to the $m = 0$ mode. This system features two eigenstates $|\Psi_\pm\rangle$ that are symmetric/anti-symmetric superpositions of the symmetric ring mode and the central donor. The anti-symmetric state can be extremely subradiant depending on the detuning Δ of the donor with respect to the ring emitters, resulting in a vanishingly small net dipole strength [23]. This leads to an optimal detuning $\Delta_{\text{sub}} \approx J_d(\tilde{\Gamma}_0 - \Gamma_0) - \tilde{J}_0$ that maximizes the subradiance of the donor with an effective decay rate $\Gamma_{\text{eff}}/\Gamma_0 \lesssim 10^{-3}$ (see Supplement 1 for details). Here, J_d is the coherent coupling between the donor and a ring emitter.

Likewise, a chain of quantum emitter rings features a rich collective eigenmode structure. In particular, the subradiance of the eigenmodes protects the excitations from radiative decoherence and leads to efficient excitation transport [15,45]. As shown above, eigenmodes of a rotationally symmetric ring carry angular momentum m. Similarly, the eigenmodes of a linear chain of quantum emitters carry linear momentum k [5,14]. This leads to an ansatz wavefunction for the eigenmodes of a ring chain, $|\Psi_{m,k}\rangle$, with an angular and linear quasi-momentum pair (m, k), and associated eigenenergies $\omega_0 + J_{m,k}$ and decay rates $\Gamma_{m,k}$ [46] (details provided in Supplement 1). The translational distance between adjacent ring centers along the chain is given by $\tilde{d} = 2R + d_R$. Figure 2(a) shows the energy bands for $N_R = 9$ and $d_R/d = 0.9$. The band structure exhibits a nontrivial topology with a non-zero Zak phase $\varphi = i \int_{BZ} dk \langle \Psi_{m=0,k} | \partial_k | \Psi_{m=0,k} \rangle$ [47] as well as gapped edge states between the energy bands of the $m = 0$ and $|m| = 1$ eigenmodes. The edge states emerge for decreasing inter-ring spacings d_R, illustrated in Fig. 2(c), and become more pronounced until a critical spacing of $d_R/d \approx 0.58$ and $d_R/d \approx 0.34$ for $N_R = 8, 9$ emitters per ring, respectively. The edge states are energetically degenerate and detuned by $\Delta_{\text{gap}}^{(0,1)}$ from the lower/upper band edge, respectively. Figure 2(b) shows the minimum distance of the edge states to the nearest band edge as a function of the inter-ring spacing d_R. Topologically protected edge states are crucial for resilient excitation transport in disordered systems [4] and $\min(\Delta_{\text{gap}}^{(0,1)})$ can serve as a figure of merit in this regard. Specifically for lattices of rings, the band gap remains finite in the presence of rotational disorder and exhibits a distinct maximum, e.g., $d_R/d \approx 0.9$ for $N_R = 9$, as shown in Fig. 2(b). Edge states also become superradiant at the critical distance where excitation transport is surpressed, as is shown in Fig. 2(c). This points to the possibility of edge mode lasing, already observed in gold nano-rings arranged in zigzag chains [19,20,48].

Figures 2(e) and 2(f) demonstrate the fundamental influence of the edge states on the transport dynamics between a donor and acceptor site for 10 rings with $N_R = 9$. At the critical spacings,

transport is either completely or strongly suppressed because the edge states possess no amplitudes in the bulk rings. Conversely, at other spacings d_R, edge states are crucial during the early times of the transport process, as demonstrated by the eigenstate fidelities $\mathcal{F}(t) = |\langle\Psi(t)|\Psi_{\rm eig}\rangle|^2$ for $N_R = 9$. Qualitatively similar results hold for other N_R. Indeed, edge states have been thoroughly studied in dimerized chains ($N_R = 2$), which reproduces a long-range generalization of the well-known Su–Schrieffer–Heeger (SSH) model [20]. A more complete discussion of the emergence of edge and corner states [48] in two-dimensional ring lattices is briefly discussed in Supplement 1 and warrants further study.

4. RESULTS: EXCITATION TRANSPORT AND TRAPPING

We now focus on the excitation transport dynamics and discuss the time evolution of a single initially excited donor. We find that excitation transport is optimized at particular donor/acceptor detunings, and that efficient transport occurs only for ring emitter numbers $N_R \geq 6$. In particular, rings with 8-, 9-, and 10-fold symmetry seem to be most optimal. This is particularly intriguing because 8-, 9-, and 10-fold rings, the most abundant type occurring in natural light harvesting antennae, show the highest resilience when rings are randomly rotated with respect to each other [49–51]. In Fig. 3, the donor excited state populations and the trap populations η_t are shown after a time $t\Gamma_0 = 150$ for a chain of 10 rings with various inter-ring spacings d_R. The detuning Δ where the donor excited state population is maximized (i.e., most subradiant) follows the optimal detuning $\Delta_{\rm sub}$ for the single-ring case. Here, the donor excitation largely remains trapped in the subradiant state discussed above, even for small inter-ring spacings.

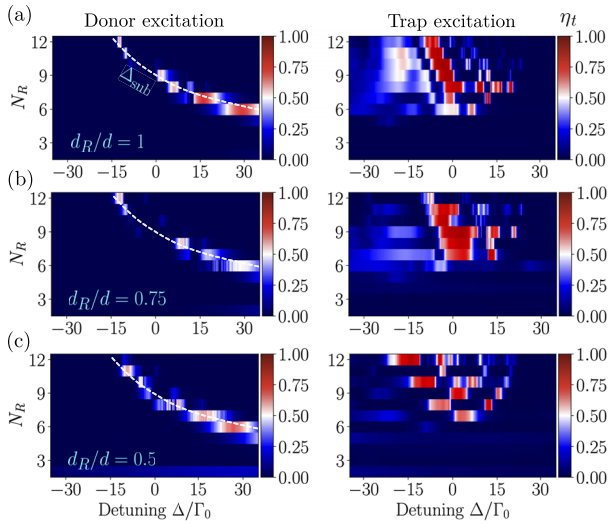

Fig. 3. (a)–(c) Excitation transport in quantum emitter rings between a donor and acceptor site. Scan over the number of emitters per ring N_R and donor/acceptor detuning Δ for 10 rings with decreasing inter-ring spacings d_R after a time $t\Gamma_0 = 150$. Efficient transport emerges only with $N_R \geq 6$, irrespective of d_R. The excited state population in the donor can get trapped in a subradiant state involving the ring surrounding the donor and follows the detuning $\Delta_{\rm sub}$ (white dashed line) derived in the main text. For 9-fold symmetric rings, the donor/acceptor detuning that optimizes transport is given by $\Delta \approx 0$ for all inter-ring spacings. Additional parameters are: $\Gamma_{\rm T} = 2\Gamma_0$, $d = 0.05\lambda_0$.

A crucial element of excitation energy transport is robustness against energy disorder. We provide a comparison of ring lattices with other lattice geometries, including the influence of static frequency disorder in the lattice emitters. This is achieved by taking emitter frequencies ω_m from a Gaussian distribution around the unperturbed emitter frequency ω_0 with a standard deviation $\delta\omega$ and adding the term $\sum_m(\omega_m - \omega_0)\hat{\sigma}_m^\dagger\hat{\sigma}_m$ to the Hamiltonian in Eq. (2). The donor/acceptor detuning Δ remains unchanged and is chosen such that unperturbed excitation transport is maximized. Figure 4 shows various geometries, many of which also have been studied previously for atoms trapped in optical lattices [4,5,10,12,21,45]. The nearest-neighbor distance is kept at $d = 0.06\lambda_0$ and the donor–acceptor distance at $\sim \lambda_0$ to establish a uniform comparison between the different geometries. Figures 4(a) and 4(b) show a hexagonal lattice with $\Delta = 0$ and a honeycomb lattice with $\Delta = 4.5\ \Gamma_0$. In Fig. 4(c), a 1D ring chain and 2D hexagonal ring lattice with $N_R = 9$ are shown with $\Delta = \Gamma_0$. The fluctuation in the emitter frequencies $\delta\omega$ is set to $|J|/4$ and $|J|/2$, where $J \approx -8.4\Gamma_0$. Altogether, the different geometries show a similar reduction in the maximal transport efficiencies under disorder but behave quite differently in the range of trapping frequencies $\Gamma_{\rm T}$ where maximal transport occurs. Whereas the hexagonal lattice exhibits peak transport at a trapping rate far above the optical decay rate, namely at $\Gamma_{\rm T}/|J| \sim 2$, the ring lattices demonstrate efficient transport over a large range $\Gamma_{\rm T}^{\rm opt}/|J| \sim 0.01$–$1$, even in the moderately disordered case. Qualitatively similar conclusions also apply to ring lattices with $N_R \neq 9$. Just as importantly, the ring lattices in Fig. 4(c) show significant transport enhancement for $\Gamma_{\rm T} \ll |J|$ compared to the independent case where no lattice is present. In summary, the ring lattices show significantly better transport capability and robustness against disorder.

So far, we have assumed that a single donor is initially excited, and we have quantified the transport behavior by calculating the fraction of the excitation that accumulates in a trap state via Eq. (1) after a waiting time t. However, in many realistic scenarios, a perfectly excited donor is rather unlikely, and emitters close to the donor will be excited too. This motivates the study of the trapping rate at which the excitation ends up in the trap state under continuous coherent illumination in the form of a Gaussian laser beam with finite beam waist w. The continuous coherent drive is modeled by

$$\hat{\mathcal{H}}_{\rm laser} = \Omega_0 \sum_i \exp\left(-\frac{|\vec{r}_d - \vec{r}_i|^2}{2w^2}\right)(\hat{\sigma}_i^\dagger + \hat{\sigma}_i), \tag{4}$$

where Ω_0 is the laser Rabi frequency and $\vec{r}_d$ is the position of the donor with the sum including all emitters. The driving rate of the laser is kept small ($\Omega_0 \ll \Gamma_0$) to ensure that the system stays in the single-excitation regime and the model remains valid. As a figure of merit for energy transport efficiency, we define $\Gamma_{\rm T}\langle\hat{\sigma}_a^\dagger\hat{\sigma}_a\rangle_{\rm st}/(4\Omega_0^2)$ as the steady-state trapping rate at the acceptor emitter. The effective trapping rate is normalized by the trapping rate of a single acceptor, given by $\sigma_0\Gamma_0\Gamma_{\rm T}/(\Gamma_0 + \Gamma_{\rm T})^2$, where $\sigma_0 = 6\pi/k_0^2$ is the single emitter scattering cross section [23]. In Figs. 5(a)–5(c), a hexagonal lattice, a honeycomb lattice, and a hexagonal ring lattice with $N_R = 9$, respectively, are compared for two laser beam waists under continuous driving. By choosing a beam waist of $w/\lambda_0 = 0.3$, most of the incoming light is focused around the donor emitter while the acceptor emitter remains mostly undriven. For $w/\lambda_0 = 3$, the whole lattice

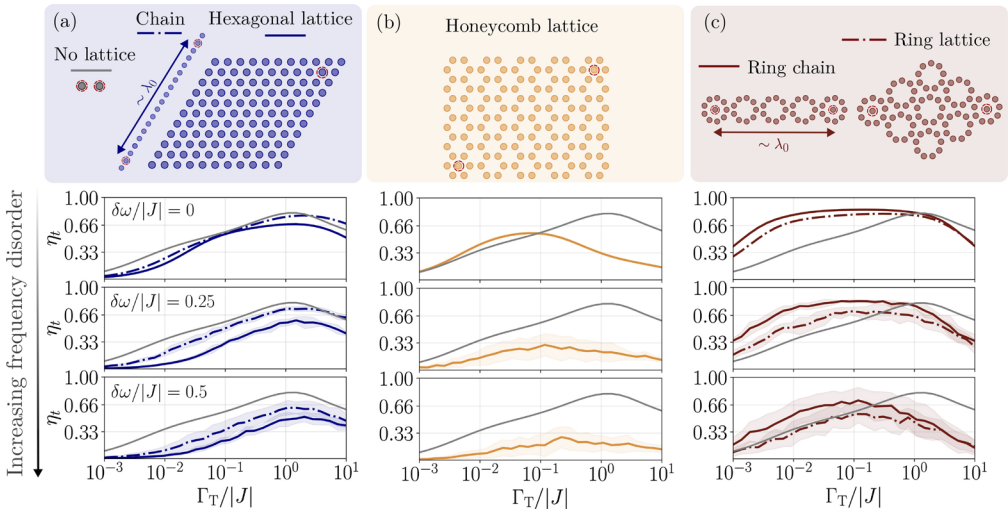

Fig. 4. Excitation transport in ring geometries exhibits superior robustness against disorder. Comparison of transport efficiency in (a) chain and hexagonal lattices and in the absence of a lattice (gray line), (b) honeycomb, and (c) ring lattices as a function of the trapping rate Γ_T and frequency disorder. Lattice emitter frequencies are randomly fluctuating by $\delta\omega$ around the resonance frequency ω_0. The donor–acceptor distance is approximately the wavelength of light λ_0. Also shown in the dash-dotted lines is the case of a donor–acceptor pair separated by d in the absence of any lattice. Although frequency disorder decreases the long-range transport capacity, it prevails remarkably well even at large frequency fluctuations. In particular, the ring lattices exhibit high transport efficiencies (close to 90%) over a wide range of trapping rates as compared to the other geometries. At trapping rates much below the magnitude of the coherent transfer rate J, ring-based lattices are superior to any other lattice in our study. Additional parameters: $d_R/d = 0.9$, $d/\lambda_0 = 0.06$, $J/\Gamma_0 \approx -8.4$, $t\Gamma_0 = 150$. An average over 25 random realizations with standard deviation $\delta\omega$ was performed in all plots. Donor/acceptor detunings of (a) $\Delta = 0$, (b) $\Delta = 4.5\Gamma_0$, and (c) $\Delta = -\Gamma_0$.

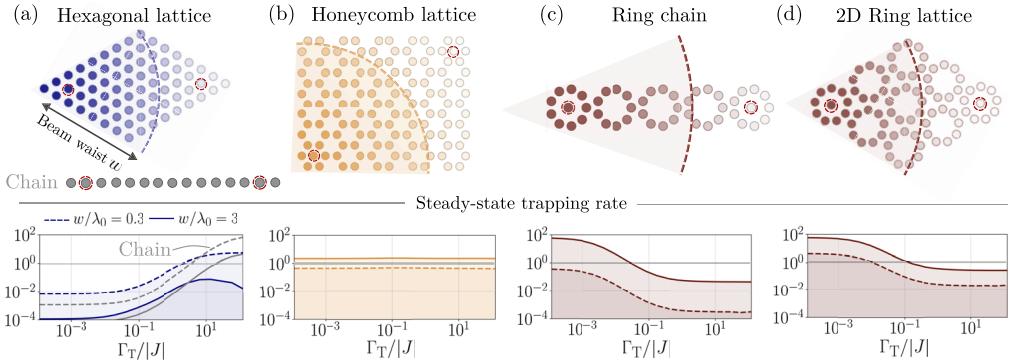

Fig. 5. Ring lattices exhibit the most efficient energy trapping under weak light illumination and small trapping rates. A comparison of the steady-state effective trapping rate $\Gamma_T\langle\hat{\sigma}_a^\dagger\hat{\sigma}_a\rangle_{st}/(4\Omega_0^2)$ between different lattice geometries under continuous coherent driving with rate $\Omega_0/\Gamma_0 = 10^{-3}$. The drive is modeled by a Gaussian beam with waist w centered at the acceptor emitter and is on-resonance with the lattice emitter frequencies ω_0 [see Eq. (4)]. The effective trapping rate is normalized by the single emitter trapping rate driven on resonance (see main text). We study a hexagonal and chain lattice in panel (a) with 20 and 8×9 emitters, a honeycomb lattice in panel (b) with 130 lattice emitters, a chain of five rings in panel (c), and a 3×3 hexagonal ring lattice in panel (d). The donor/acceptor distance is approximately the wavelength of light λ_0 in all lattices. Strikingly, only the ring-based lattices are orders of magnitude more efficient at trapping incoming light for trapping rates below the nearest-neighbor coupling rate, namely when $\Gamma_T \ll |J|$. Conversely, the honeycomb and hexagonal lattices are orders of magnitude less efficient in the same regime with the honeycomb lattice not deviating significantly from the single acceptor case. The linear chain (gray dashed) and the free space transfer (solid gray) shown in panel (a) is more efficient at trapping rates $\Gamma_T > |J|$. Additional parameters: $d/\lambda_0 = 0.06$, $J/\Gamma_0 \approx -8.4$ and donor/acceptor detunings of (a) $\Delta/\Gamma_0 = -18$ (hexagonal), $\Delta = 0$ (chain), (b) $\Delta/\Gamma_0 = -20$, (c) $\Delta/\Gamma_0 = -3.85$, (d) $\Delta/\Gamma_0 = -4.63$ with $d_R/d = 0.9$, $N_R = 9$, in panels (c) and (d).

is uniformly driven—a scenario more applicable to deeply sub-wavelength lattices under illumination from a non-directional light source. Natural light-harvesting antennae in purple bacteria offer an example [24]. In all cases, the donor/acceptor detuning Δ is chosen optimally such that the trapping rate is maximized. We find that the ring lattice is many orders of magnitude more efficient in trapping incident light as compared to both the triangular and honeycomb lattices as well as the single emitter at trapping rates much below the nearest-neighbor coherent transfer rate J. In particular, for $\Gamma_T/|J| \lesssim 0.01$, the ring lattice exhibits an almost 100× higher trapping efficiency compared to an independent emitter and the other lattices.

5. CONCLUSIONS

In conclusion, we have demonstrated intriguing optical properties of quantum emitter ring lattices, including the emergence of topological edge states. Furthermore, we have shown based on general symmetry principles that ring lattices form a superior platform for transporting and trapping excitations. We have also elucidated the guiding principles that govern optimal donor/acceptor detunings, trapping rates, and geometric arrangements with robustness against static energy disorder. Under more realistic conditions of weak coherent light illumination, we have shown that ring lattices are orders of magnitude more efficient at trapping the absorbed light when the trapping rate is much smaller than the nearest-neighbor coherent coupling rate. This result is thought-provoking since natural light-harvesting systems also operate with trapping mechanisms that are orders of magnitude slower than the coherent transfer time between neighboring chromophores [52,53]. Measurements performed on natural light-harvesting complexes show that the coherent energy transfer time between neighboring chromophores during photosynthesis is of the order of ~ 0.1–10 ps whereas the trapping time in the reaction center is typically ~ 0.1–10 ns [35,52,53]. For a pre-existing trapping structure, this could provide an explanation why nature uses ring geometries as a moderating mechanism to trap absorbed sun light in reaction centers. Other studies have focused on molecular emitters in ambient conditions with vibrational degrees of freedom as well as multiple decoherence channels [54–56]. These works have shown that coupling between electronic and vibronic modes can aid the transport and trapping processes in ordered molecular arrays such as ring geometries via unidirectional transfer from superradiant to subradiant collective electronic states [57–59]. The impact of these additional effects on the results presented here are an exciting avenue for future research [60–62]. Nevertheless, our results suggest that there exist general and platform-agnostic design principles that govern the efficient transport of excitation energy at the nano scale. These geometrical considerations may have played a role in evolutionary design and warrant further study.

Funding. Austrian Science Fund (DK-ALM W1259-N27); Harvard Quantum Initiative (HQI); AFOSR and the NSF (through the CUA PFC and QSense QLCI).

Disclosures. The authors declare no conflicts of interest.

Data availability. Data underlying the results presented in this paper are not publicly available at this time but may be obtained from the authors upon reasonable request.

Supplemental document. See Supplement 1 for supporting content.

REFERENCES

1. R. Bekenstein, I. Pikovski, H. Pichler, *et al.*, "Quantum metasurfaces with atom arrays," Nat. Phys. **16**, 676–681 (2020).
2. J. Rui, D. Wei, A. Rubio-Abadal, *et al.*, "A subradiant optical mirror formed by a single structured atomic layer," Nature **583**, 369–374 (2020).
3. M. T. Manzoni, M. Moreno-Cardoner, A. Asenjo-Garcia, *et al.*, "Optimization of photon storage fidelity in ordered atomic arrays," New J. Phys. **20**, 083048 (2018).
4. J. Perczel, J. Borregaard, D. E. Chang, *et al.*, "Topological quantum optics in two-dimensional atomic arrays," Phys. Rev. Lett. **119**, 023603 (2017).
5. S. J. Masson and A. Asenjo-Garcia, "Atomic-waveguide quantum electrodynamics," Phys. Rev. Res. **2**, 043213 (2020).
6. R. Gutiérrez-Jáuregui and A. Asenjo-Garcia, "Coherent control in atomic chains: to trap and release a traveling excitation," Phys. Rev. Res. **4**, 013080 (2022).
7. H. H. Jen, M. S. Chang, and Y. C. Chen, "Cooperative light scattering from helical-phase-imprinted atomic rings," Sci. Rep. **8**, 9570 (2018).
8. P.-O. Guimond, A. Grankin, D. V. Vasilyev, *et al.*, "Subradiant bell states in distant atomic arrays," Phys. Rev. Lett. **122**, 093601 (2019).
9. M. Reitz, C. Sommer, and C. Genes, "Cooperative quantum phenomena in light-matter platforms," PRX Quantum **3**, 010201 (2022).
10. T. L. Patti, D. S. Wild, E. Shahmoon, *et al.*, "Controlling interactions between quantum emitters using atom arrays," Phys. Rev. Lett. **126**, 223602 (2021).
11. E. Shahmoon, D. S. Wild, M. D. Lukin, *et al.*, "Cooperative resonances in light scattering from two-dimensional atomic arrays," Phys. Rev. Lett. **118**, 113601 (2017).
12. S. Buckley-Bonanno, S. Ostermann, O. Rubies-Bigorda, *et al.*, "Optimized geometries for cooperative photon storage in an impurity coupled to a two-dimensional atomic array," Phys. Rev. A **106**, 053706 (2022).
13. M. Gross and S. Haroche, "Superradiance: an essay on the theory of collective spontaneous emission," Phys. Rep. **93**, 301–396 (1982).
14. A. Asenjo-Garcia, M. Moreno-Cardoner, A. Albrecht, *et al.*, "Exponential improvement in photon storage fidelities using subradiance and "selective radiance" in atomic arrays," Phys. Rev. X **7**, 031024 (2017).
15. J. A. Needham, I. Lesanovsky, and B. Olmos, "Subradiance-protected excitation transport," New J. Phys. **21**, 073061 (2019).
16. M. Moreno-Cardoner, D. Goncalves, and D. E. Chang, "Quantum nonlinear optics based on two-dimensional rydberg atom arrays," Phys. Rev. Lett. **127**, 263602 (2021).
17. R. J. Bettles, S. A. Gardiner, and C. S. Adams, "Enhanced optical cross section via collective coupling of atomic dipoles in a 2D array," Phys. Rev. Lett. **116**, 103602 (2016).
18. N. Aslam, H. Zhou, E. K. Urbach, *et al.*, "Quantum sensors for biomedical applications," Nat. Rev. Phys. **5**, 157–169 (2023).
19. M. Parto, S. Wittek, H. Hodaei, *et al.*, "Edge-mode lasing in 1D topological active arrays," Phys. Rev. Lett. **120**, 113901 (2018).
20. P. St-Jean, V. Goblot, E. Galopin, *et al.*, "Lasing in topological edge states of a one-dimensional lattice," Nat. Photonics **11**, 651–656 (2017).
21. M. Moreno-Cardoner, D. Plankensteiner, L. Ostermann, *et al.*, "Subradiance-enhanced excitation transfer between dipole-coupled nanorings of quantum emitters," Phys. Rev. A **100**, 023806 (2019).
22. R. Holzinger, D. Plankensteiner, L. Ostermann, *et al.*, "Nanoscale coherent light source," Phys. Rev. Lett. **124**, 253603 (2020).
23. M. Moreno-Cardoner, R. Holzinger, and H. Ritsch, "Efficient nanophotonic antennas based on dark states in quantum emitter rings," Opt. Express **30**, 10779–10791 (2022).
24. G. D. Scholes, G. R. Fleming, A. Olaya-Castro, *et al.*, "Lessons from nature about solar light harvesting," Nat. Chem. **3**, 763–774 (2011).
25. A. Olaya-Castro, C. F. Lee, F. F. Olsen, *et al.*, "Efficiency of energy transfer in a light-harvesting system under quantum coherence," Phys. Rev. B **78**, 085115 (2008).
26. A. Mattioni, F. Caycedo-Soler, S. F. Huelga, *et al.*, "Design principles for long-range energy transfer at room temperature," Phys. Rev. X **11**, 041003 (2021).
27. F. Levi, S. Mostarda, F. Rao, *et al.*, "Quantum mechanics of excitation transport in photosynthetic complexes: a key issues review," Rep. Prog. Phys. **78**, 082001 (2015).
28. M. Escalante, A. Lenferink, Y. Zhao, *et al.*, "Long-range energy propagation in nanometer arrays of light harvesting antenna complexes," Nano Lett. **10**, 1450–1457 (2010). PMID: 20232894.
29. G. Panitchayangkoon, D. V. Voronine, D. Abramavicius, *et al.*, "Direct evidence of quantum transport in photosynthetic light-harvesting complexes," Proc. Natl. Acad. Sci. U. S. A. **108**, 20908–20912 (2011).
30. H. Lee, Y.-C. Cheng, and G. R. Fleming, "Coherence dynamics in photosynthesis: protein protection of excitonic coherence," Science **316**, 1462–1465 (2007).

31. C. Creatore, M. A. Parker, S. Emmott, *et al.*, "Efficient biologically inspired photocell enhanced by delocalized quantum states," Phys. Rev. Lett. **111**, 253601 (2013).
32. J. Strümpfer, M. Sener, and K. schulten, "How quantum coherence assists photosynthetic light-harvesting," J. Phys. Chem. Lett. **3**, 536–542 (2012). PMID: 22844553.
33. A. Potočnik, A. Bargerbos, F. A. Y. N. Schröder, *et al.*, "Studying light-harvesting models with superconducting circuits," Nat. Commun. **9**, 904 (2018).
34. F. Fassioli, R. Dinshaw, P. C. Arpin, *et al.*, "Photosynthetic light harvesting: excitons and coherence," J. R. Soc. Interface. **11**, 20130901 (2014).
35. T. Mirkovic, E. E. Ostroumov, J. M. Anna, *et al.*, "Light absorption and energy transfer in the antenna complexes of photosynthetic organisms," Chem. Rev. **117**, 249–293 (2017).
36. J. S. Peter, R. Holzinger, S. Ostermann, *et al.*, Manuscript in preparation (2023).
37. F. Caycedo-Soler, F. J. Rodríguez, L. Quiroga, *et al.*, "Light-harvesting mechanism of bacteria exploits a critical interplay between the dynamics of transport and trapping," Phys. Rev. Lett. **104**, 158302 (2010).
38. R. Ranjbar Choubeh, R. B. Koehorst, D. Bína, *et al.*, "Efficiency of excitation energy trapping in the green photosynthetic bacterium chlorobaculum tepidum," Biochim. Biophys. Acta, Bioenerg. **1860**, 147–154 (2019).
39. K. Timpmann, M. Chenchiliyan, E. Jalviste, *et al.*, "Efficiency of light harvesting in a photosynthetic bacterium adapted to different levels of light," Biochim. Biophys. Acta, Bioenerg. **1837**, 1835–1846 (2014).
40. J.-L. Brédas, E. H. Sargent, and G. D. Scholes, "Photovoltaic concepts inspired by coherence effects in photosynthetic systems," Nat. Mater. **16**, 35–44 (2017).
41. C. M. Kropf, A. Valli, P. Franceschini, *et al.*, "Towards high-temperature coherence-enhanced transport in heterostructures of a few atomic layers," Phys. Rev. B **100**, 035126 (2019).
42. G. M. Akselrod, P. B. Deotare, N. J. Thompson, *et al.*, "Visualization of exciton transport in ordered and disordered molecular solids," Nat. Commun. **5**, 3646 (2014).
43. S. K. Saikin, A. Eisfeld, S. Valleau, *et al.*, "Photonics meets excitonics: natural and artificial molecular aggregates," Nanophotonics **2**, 21–38 (2013).
44. G. L. Celardo, P. Poli, L. Lussardi, *et al.*, "Cooperative robustness to dephasing: single-exciton superradiance in a nanoscale ring to model natural light-harvesting systems," Phys. Rev. B **90**, 085142 (2014).
45. K. E. Ballantine and J. Ruostekoski, "Subradiance-protected excitation spreading in the generation of collimated photon emission from an atomic array," Phys. Rev. Res. **2**, 023086 (2020).
46. A. Albrecht, L. Henriet, A. Asenjo-Garcia, *et al.*, "Subradiant states of quantum bits coupled to a one-dimensional waveguide," New J. Phys. **21**, 025003 (2019).
47. B. A. Bernevig, *Topological Insulators and Topological Superconductors* (Princeton University Press, 2013).
48. Y. Ota, K. Takata, T. Ozawa, *et al.*, "Active topological photonics," Nanophotonics **9**, 547–567 (2020).
49. S. Scheuring and J. N. Sturgis, "Atomic force microscopy of the bacterial photosynthetic apparatus: plain pictures of an elaborate machinery," Photosynth. Res. **102**, 197–211 (2009).
50. L. Cleary, H. Chen, C. Chuang, *et al.*, "Optimal fold symmetry of LH2 rings on a photosynthetic membrane," Proc. Natl. Acad. Sci. U. S. A. **110**, 8537–8542 (2013).
51. X. Hu, A. Damjanovic, T. Ritz, *et al.*, "Architecture and mechanism of the light-harvesting apparatus of purple bacteria," Proc. Natl. Acad. Sci. U. S. A. **95**, 5935–5941 (1998).
52. H. C. Chan, O. E. Gamel, G. R. Fleming, *et al.*, "Single-photon absorption by single photosynthetic light-harvesting complexes," J. Phys. B: At. Mol. Opt. Phys. **51**, 054002 (2018).
53. R. van Grondelle, J. P. Dekker, T. Gillbro, *et al.*, "Energy transfer and trapping in photosynthesis," Biochim. Biophys. Acta, Bioenerg. **1187**, 1–65 (1994).
54. M. Mohseni, P. Rebentrost, S. Lloyd, *et al.*, "Environment-assisted quantum walks in photosynthetic energy transfer," J. Chem. Phys. **129**, 174106 (2008).
55. M. B. Plenio and S. F. Huelga, "Dephasing-assisted transport: quantum networks and biomolecules," New J. Phys. **10**, 113019 (2008).
56. N. Werren, W. Brown, and E. M. Gauger, "Light harvesting enhanced by quantum ratchet states," PRX Energy **2**, 013002 (2023).
57. S. Davidson, F. A. Pollock, and E. Gauger, "Eliminating radiative losses in long-range exciton transport," PRX Quantum **3**, 020354 (2022).
58. W. M. Brown and E. M. Gauger, "Light harvesting with guide-slide superabsorbing condensed-matter nanostructures," J. Phys. Chem. Lett. **10**, 4323–4329 (2019).
59. R. Holzinger, S. A. Oh, M. Reitz, *et al.*, "Cooperative subwavelength molecular quantum emitter arrays," Phys. Rev. Res. **4**, 033116 (2022).
60. J. Cao, R. J. Cogdell, D. F. Coker, *et al.*, "Quantum biology revisited," Sci. Adv. **6**, eaaz4888 (2020).
61. S. Kundu, R. Dani, and N. Makri, "Tight inner ring architecture and quantum motion of nuclei enable efficient energy transfer in bacterial light harvesting," Sci. Adv. **8**, eadd0023 (2022).
62. D. Palecek, P. Edlund, S. Westenhoff, *et al.*, "Quantum coherence as a witness of vibronically hot energy transfer in bacterial reaction center," Sci. Adv. **3**, e1603141 (2017).